

Higher-order accurate two-sample network inference and network hashing

Meijia Shao[†], Dong Xia^{§*}, Yuan Zhang[†], Qiong Wu[#] and Shuo Chen[‡]

[†] The Ohio State University

[§] Hong Kong Univeristy of Science and Technology

[#] University of Pennsylvania

[‡] University of Maryland

August 17, 2022

Abstract

Two-sample hypothesis testing for comparing two networks is an important yet difficult problem. Major challenges include: potentially different sizes and sparsity levels; non-repeated observations of adjacency matrices; computational scalability; and theoretical investigations, especially on finite-sample accuracy and minimax optimality. In this article, we propose the first provably higher-order accurate two-sample inference method by comparing network moments. Our method extends the classical two-sample t-test to the network setting. We make weak modeling assumptions and can effectively handle networks of different sizes and sparsity levels. We establish strong finite-sample theoretical guarantees, including rate-optimality properties. Our method is easy to implement and computes fast. We also devise a novel nonparametric framework of offline hashing and fast querying particularly effective for maintaining and querying very large network databases. We demonstrate the effectiveness of our method by comprehensive simulations. We apply our method to two real-world data sets and discover interesting novel structures.

Keywords— Network analysis, two-sample test, Edgeworth expansion, network hashing, non-parametric inference

1 Introduction

The relational nature of network data presents unique challenges to data analysts. It is therefore very intriguing to ask how to extend statistical concepts, tools and theory in the classical i.i.d. setting to network settings. Levin and Levina (2019) said well: “*A core problem in statistical network*

*Dong Xia’s research was partially supported by Hong Kong RGC grant ECS 26302019.

analysis is to develop network analogues of classical techniques.” Indeed, recent years witnessed significant developments of network analysis toolbox for both point estimation (Abbe, 2017) and one-sample inference (Gao and Lafferty, 2017; Banerjee and Ma, 2017; Green and Shalizi, 2022; Jin et al., 2018; Levin and Levina, 2019; Zhang and Xia, 2022). Comprehensive theoretical analysis of these tools deepened our understanding of their behaviors and performances.

This paper studies a challenging and under-explored topic: two-sample network comparison. Spoken in plain language, the scientific question is how to compare two network models \mathcal{F}_A and \mathcal{F}_B based on their respective observations $A^{(1)}, \dots, A^{(N_A)}$ and $B^{(1)}, \dots, B^{(N_B)}$. Though being challenging in general, this problem can be made easier by imposing two popular assumptions. The first popular assumption is repeated network observations, that is, $N_A, N_B \geq 2$ and possibly even diverge, such as Ginestet et al. (2017); Ghoshdastidar and Von Luxburg (2018); Kolaczyk et al. (2020); Ghoshdastidar et al. (2020); Chen et al. (2022b); Maugis et al. (2020); Bravo-Hermesdorff et al. (2021); Yuan and Wen (2021). This assumption is particularly strong in that it implicitly assumes repeated network observations within each group are identically distributed. However, many real-world data sets clearly exhibit within-group heterogeneity, see Section 5.5. Methods designed under this assumption will not be able to discover within-group heterogeneity. The second popular assumption states that all networks share a common node set, with known node correspondence, including Ghoshdastidar and Von Luxburg (2018); Li and Li (2018); Ghoshdastidar et al. (2020); Chen et al. (2022b). This assumption is sensible in some applications such as networks between the same set of participants, but it is restrictive in general. Two-sample network comparison becomes most challenging in the absence of the aforementioned two assumptions, namely, $N_A = N_B = 1$ and there is no available node correspondence. Prior works typically require additional strong structural assumptions such as low-rankness or strict degree monotonicity (Tang et al., 2017; Agterberg et al., 2020; Yang et al., 2014; Sabanayagam et al., 2021).

In this paper, we address the most challenging version of this problem without strong modeling assumptions, with three further scientific considerations in mind. First, one might be more interested in learning some key numerical features of a population than learning its every detail. This is an eminent philosophy featured by method-of-moments in classical statistics, but not much reflected in existing network analysis literature, possibly due to technical challenges. Second, we pay close attention to computational speed. The two-sample t-test in the classical i.i.d. setting can be computed using a few statistics of the two samples, respectively, without using the raw data; in stark contrast, most existing network two-sample inference tools require expensive computation of some cross-terms based on two adjacency matrices (Ghoshdastidar et al., 2017; Agterberg et al., 2020). Third, we are particularly interested in quantifying the statistical limit of this problem. That is to answer the question: for each given configuration of network sizes and sparsity levels, how different should the two network moments be, in order to be distinguishable?

The highlights of our paper are as follows. On the methodology side, first, our method does not require repeated network observations, parametric model assumption, or known node registration, making it widely applicable and versatile. Second, we compare moments, as important numerical features of two networks, not necessarily whether the two network models are identical in every aspect. Third, our method breaks down the two-sample test into two stages: a novel network hashing method in the first stage, where we offline hash each networks into a short vector of summary

statistics. In the second stage we perform the test using only the summary statistics without further needing the adjacency matrices. This novel tool not only greatly speeds up comparison among a large pair of networks, but also improves data privacy protection since each network only needs to supply its summary statistics. On the theory side, our method enjoys several strong theoretical guarantees. First, our method is provably effective for networks of very different sizes and sparsity levels and can handle a much wider range of parameters than existing literature (Agterberg et al., 2020). Second, our inference procedure enjoys higher-order accuracy under mild conditions, which is new in literature to our best knowledge. Third, our method enjoys minimax optimality that we shall elaborate in Theorem 3. No akin result exists to our best knowledge.

2 Graphon Model and Network Moments

2.1 Two-sample graphon model

For narrative simplicity, we state our method and theory for unweighted, undirected networks with no self-loop, but these specifications are not essential. We observe two independent networks with m and n nodes, respectively, represented by their adjacency matrices $A \in \{0, 1\}^{m \times m}$ and $B \in \{0, 1\}^{n \times n}$, where $A = A^T, B = B^T, \text{diag}(A) = 0$ and $\text{diag}(B) = 0$. Throughout this paper, we choose graphon model as our base model. Graphon is a very general wrapper around many famous and widely-used network models, including stochastic block models (Gao et al., 2018), random dot-product models (Young and Scheinerman, 2007), exponential random graph models (Hunter et al., 2008), general smooth networks (Bickel and Chen, 2009; Olhede and Wolfe, 2014) and so on. Our method, though designed to work for graphons, also works for these models as special cases. The data generation mechanism is as follows. First, assign a latent position to each node: $X_1, \dots, X_m, Y_1, \dots, Y_n \stackrel{i.i.d.}{\sim} \text{Uniform}[0, 1]$. Second, there exists a latent, symmetric graphon function $f_A(\cdot, \cdot) : [0, 1]^2 \rightarrow \mathbb{R}^+$ encoding all network structures, and a sparsity parameter ρ_A , such that the edge probability between (i_1, i_2) is $W_{i_1, i_2}^{(A)} = \rho_A \cdot f_A(X_{i_1}, X_{i_2})$. We inherit the regularity condition for model identifiability $\int_{[0, 1]^2} f_A(u, v) du dv = 1$ from Olhede and Wolfe (2014). Similarly define ρ_B and $f_B(\cdot, \cdot)$. Finally, our observation A is generated according to $\mathbb{P}(A_{i_1, i_2} = A_{i_2, i_1} = 1) = W_{i_1, i_2}^{(A)}$ for all $1 \leq i_1 < i_2 \leq m$. Similarly define $\rho_B, f_B(\cdot, \cdot), W^{(B)}$ and generate B . General audience may wonder if one can estimate f_A, f_B, X 's and Y 's and use them to compare network structures. Unfortunately, f_A, f_B are only identifiable up to equivalent classes (Olhede and Wolfe, 2014; Gao et al., 2015; Zhang et al., 2017). The edge probability matrices $W^{(A)}, W^{(B)}$ are fully identifiable, so one naturally considers a graph-matching-based network comparison. However, graph matching is a difficult problem even with structural assumptions (Lyzinski et al., 2015; Arroyo et al., 2021), and it typically requires rather costly computation.

2.2 Network method of moments

Our approach is to compare network moments, namely, the frequencies of patterned motifs, e.g. edges, triangles, star-shapes and circles (Bickel et al., 2011; Jin et al., 2018; Levin and Levina, 2019). The idea is naturally inspired by its counterpart in classical statistics, where we compare the means,

variances and other numerical features of two populations. Network method of moments enjoys high computational speed and memory efficiency (Zhang and Xia, 2022). Particularly conveniently, they are invariant under node permutations, which exempts our approach from a slow and difficult graph matching step and easily enables it to handle different network sizes. Interestingly, two potentially very different network models may still share some common numerical features of scientific importance and interest. This is exactly analogous to the understanding for moments in the i.i.d. setting. By Borgs et al. (2010), knowing all moments can nearly determine the network population distribution. Therefore, our proposed toolbox features a unique flexibility, in that our method can be used to either compare only some selected moments of the two networks, which two might be very different in some other moments; or to effectively compare their entire population distributions by comparing many moments.

Now we formally define network moments. Let R denote a given motif of r nodes and s edges. Throughout this paper, we always assume the motif R is connected. Following the tradition of Bickel et al. (2011); Zhang and Xia (2022); Maugis et al. (2020), define

$$h(A_0) := \begin{cases} 1 & \exists \text{ bijection } \pi : [1 : r] \leftrightarrow [1 : r], \text{ s.t. } (A_0)_{i,j} \geq R_{\pi(i)\pi(j)}, \forall 1 \leq i < j \leq r, \\ 0 & \text{otherwise,} \end{cases} \quad (1)$$

for any r -node graph A_0 . The empirical network moment indexed by R for network A is $\hat{U}_m := \binom{m}{r}^{-1} \sum_{1 \leq i_1 < \dots < i_r \leq m} h(A_{i_1, \dots, i_r})$, where we omit the dependency of h and \hat{U}_m on R to simplify notation. Here $A_{\mathcal{I}}$ denotes the sub-matrix with row and column indices from the set \mathcal{I} . Denote the corresponding population moment by $\mu_m := \mathbb{E}[\hat{U}_m]$, where the expectation is taken w.r.t. the randomness of both network edges and latent positions. Similarly define \hat{V}_n and ν_n for network B . Notice that, however, the moments $\hat{U}_m, \mu_m, \hat{V}_n, \nu_n$ are impacted by network sparsity measures $\rho_A, \hat{\rho}_A, \rho_B$ and $\hat{\rho}_B$, respectively, where define $\hat{\rho}_A := \binom{m}{2}^{-1} \sum_{1 \leq i_1 < i_2 \leq m} A_{i_1 i_2}$ and $\hat{\rho}_B$ similarly. Networks may exhibit very different sparsity levels (Decelle et al., 2011). To rule out the nuisance of network sparsity, similar to Bickel et al. (2011); Bhattacharya et al. (2022), we consider the Horvitz–Thompson estimators when designing the population discrepancy measure d_{m,n,ρ_A,ρ_B} , defined as

$$d_{m,n,\rho_A,\rho_B} := \rho_A^{-s} \cdot \mu_m - \rho_B^{-s} \cdot \nu_n.$$

Our central goal is to perform inference on d_{m,n,ρ_A,ρ_B} . A natural point estimator of d_{m,n,ρ_A,ρ_B} is

$$\hat{D}_{m,n} := \hat{\rho}_A^{-s} \cdot \hat{U}_m - \hat{\rho}_B^{-s} \cdot \hat{V}_n.$$

The main task is then to characterize the distribution of $\hat{D}_{m,n}$.

3 Higher-order Accurate Method by Edgeworth Expansion

3.1 Estimating $\text{Var}(\hat{D}_{m,n})$ and designing the studentization $\hat{T}_{m,n}$

We quickly outline this section’s contents. We first estimate $\text{Var}(\hat{D}_{m,n})$ and use it to studentize $\hat{D}_{m,n}$; this is nontrivial as variance estimators that require repeated network observations such as

Maugis et al. (2020); Bravo-Hermsdorff et al. (2021) cannot function here. Then we studentize $\widehat{D}_{m,n}$ and formulate a higher-order accurate distributional approximation. This formulation then leads to our novel network offline hashing and fast querying toolbox. We also formulate the Cornish-Fisher confidence interval by inverting the CDF approximation. We conclude this section with our theorems that establish finite-sample accuracy and minimax optimality.

We now brief the rationale in our designed estimator of $\text{Var}(\widehat{D}_{m,n})$. Readers not interested in technical details may skip to eq. (2). To estimate $\text{Var}(\widehat{D}_{m,n})$, we decompose the stochastic variation in $\widehat{\rho}_A^{-s} \cdot \widehat{U}_m$ as follows: $\widehat{\rho}_A^{-s} \cdot \widehat{U}_m = \{\rho_A + (\widetilde{\rho}_A - \rho_A) + (\widehat{\rho}_A - \widetilde{\rho}_A)\}^{-s} \cdot \{\mu_m + (\widetilde{U}_m - \mu_m) + (\widehat{U}_m - \widetilde{U}_m)\}$, where we define $\widetilde{\rho}_A := \mathbb{E}[\widehat{\rho}_A | X_1, \dots, X_m]$ and $\widetilde{U}_m := \mathbb{E}[\widehat{U}_m | X_1, \dots, X_m]$. Random variables $\widetilde{\rho}_A$ and \widetilde{U}_m are classical noiseless U-statistics of degrees 2 and r , respectively. Their randomness is exclusively driven by X_1, \dots, X_m ; thus they admit Hoeffding's decompositions (Hoeffding, 1948): $\widetilde{U}_m = \mu_m + (r/m) \sum_{i=1}^m g_{A;1}(X_i) + \widetilde{O}_p(\rho_A^s m^{-1} \log m)$ and $\widetilde{\rho}_A = \rho_A + (2/m) \sum_{i=1}^m g_{\rho_A;1}(X_i) + \widetilde{O}_p(\rho_A m^{-1} \log m)$, respectively, where we slightly abuse notation and write $h(X_1, \dots, X_r) := \mathbb{E}[h(A_{1,\dots,r}) | X_1, \dots, X_r]$, define $g_{A;1}(X_1) := \mathbb{E}[h(X_1, \dots, X_r) | X_1] - \mu_m$, $g_{\rho_A;1}(X_1) := \rho_A \cdot \mathbb{E}[f_A(X_1, X_2) | X_1] - \rho_A$, and write $a_{m,n} = \widetilde{O}_p(b_{m,n})$ if $\mathbb{P}(|a_{m,n}/b_{m,n}| \geq C) = O((m \wedge n)^{-1})$ for some constant $C > 0$. It turns out that when $\rho_A \gg m^{-1}$, $\rho_B \gg n^{-1}$, the variation contributed by $\widehat{\rho}_A - \widetilde{\rho}_A$ and $\widehat{U}_m - \widetilde{U}_m$ are dominated by that in $\widetilde{\rho}_A - \rho_A$ and $\widetilde{U}_m - \mu_m$. Here, terms $\widehat{\rho}_A - \widetilde{\rho}_A$ and $\widehat{U}_m - \widetilde{U}_m$ are both dominated by a weighted average of $\eta_{ij}^{(A)} := A_{ij} - W_{ij}^{(A)}$ terms, and $\widehat{U}_m - \widetilde{U}_m$ contains a $\widetilde{O}_p(\rho_A^{-1/2} m^{-1} \log^{1/2} m)$ remainder term while $\widehat{\rho}_A - \widetilde{\rho}_A$ does not. Putting these understandings together, we have

$$\widehat{\rho}_A^{-s} \cdot \widehat{U}_m = \rho_A^{-s} \mu_m + \frac{1}{m} \sum_{i=1}^m \alpha_1(X_i) + \widetilde{O}_p(\rho_A^{-1/2} \cdot m^{-1} \log^{1/2} m + m^{-1} \log m). \quad (2)$$

where $\alpha_1(X_i) := r \rho_A^{-s} g_{A;1}(X_i) - 2s \rho_A^{-(s+1)} \mu_m g_{\rho_A;1}(X_i)$. The B -index counterparts $g_{B;1}(Y_i)$ and $g_{\rho_B;1}(Y_i)$ are defined in the same fashion. Eq. (2) is the foundation for us to estimate the variance of $\widehat{\rho}_A^{-s} \cdot \widehat{U}_m$.

We set $\rho_A \gg m^{-1}$ throughout this paper, so $\text{Var}(\widehat{\rho}_A^{-s} \cdot \widehat{U}_m) \approx m^{-1} \text{Var}(\alpha_1(X_1)) \approx m^{-2} \sum_{i=1}^m \widehat{\alpha}_1^2(X_i)$, where we design $\widehat{\alpha}_1(X_i) := r \widehat{\rho}_A^{-s} \widehat{g}_{A;1}(X_i) - 2s \widehat{\rho}_A^{-(s+1)} \widehat{U}_m \widehat{g}_{\rho_A;1}(X_i)$, with $\widehat{g}_{A;1}(X_i) := \binom{m-1}{r-1}^{-1} \sum_{\{i_1 < \dots < i_m\} \subseteq [1:m] \setminus \{i\}} h(A_{i,i_1,\dots,i_{r-1}}) - \widehat{U}_m$ and $\widehat{g}_{\rho_A;1}(X_i) := (m-1)^{-1} \sum_{1 \leq i' \leq m, i' \neq i} A_{ii'} - \widehat{\rho}_A$. Similarly define the B -indexed counterparts $\beta_1(Y_i)$ and $\widehat{\beta}_1(Y_j)$. We estimate $\text{Var}(\widehat{D}_{m,n}) \approx \sigma_{m,n}^2 := m^{-1} \mathbb{E}[\alpha_1^2(X_1)] + n^{-1} \mathbb{E}[\beta_1^2(Y_1)]$ by

$$\widehat{S}_{m,n}^2 := m^{-2} \sum_{i=1}^m \widehat{\alpha}_1^2(X_i) + n^{-2} \sum_{j=1}^n \widehat{\beta}_1^2(Y_j). \quad (3)$$

Now we are ready to studentize $\widehat{D}_{m,n}$ as follows

$$\widehat{T}_{m,n} := \widehat{S}_{m,n}^{-1} \cdot \{\widehat{D}_{m,n} - (\rho_A^{-s} \cdot \mu_m - \rho_B^{-s} \cdot \nu_n)\}. \quad (4)$$

One can equivalently use jackknife (Maesono, 1997) to design $\widehat{S}_{m,n}$, but our design is more convenient for analysis; see Theorem 3.3 in Zhang and Xia (2022) and the paragraph beneath it.

3.2 Characterizing the distribution of $\widehat{T}_{m,n}$

In this section, we present Edgeworth expansions as a higher-order accurate means to approximate the c.d.f. $F_{\widehat{T}_{m,n}}$. To start, we set up some auxiliary quantities as building bricks of the coefficients in our expansion formula. Define the second-order terms in Hoeffding decomposition $g_{A;2}(X_1, X_2) := \mathbb{E}[h(X_1, \dots, X_r)|X_1, X_2] - g_{A;1}(X_1) - g_{A;1}(X_2) - \mu_m$, and similarly define $g_{\rho_A;2}(X_1, X_2)$; also set $\xi_{A;1}^2 := \text{Var}(g_{A;1}(X_1))$, $\xi_{\rho_A;1}^2 := \text{Var}(g_{\rho_A;1}(X_1))$ and $\xi_{A,\rho_A;1} := \mathbb{E}[g_{A;1}(X_1)g_{\rho_A;1}(X_1)]$. Recall we defined $\alpha_1(X_i)$ in Section 3.1 and define auxiliary quantities α_0 , $\alpha_2(X_{i_1}, X_{i_2})$, $\alpha_3(X_i)$ and $\alpha_4(X_{i_1}, X_{i_2})$, $1 \leq \{i; i_1 < i_2\} \leq m$. Due to page limit, we sink their definitions to Section S.1 in Supplementary Material. Define $\xi_{B;1}^2$, $\xi_{\rho_B;1}^2$, $\xi_{B,\rho_B;1}$, β_0 , β_2 through β_4 similarly for graphon B . Set

$$\begin{aligned} \mathcal{I}_0 &:= \sigma_{m,n}^{-1}(m^{-1}\alpha_0 - n^{-1}\beta_0), \\ Q_{m,n,\rho_A,\rho_B;1} &:= \frac{1}{2}\sigma_{m,n}^{-3} \left\{ -m^{-2}\mathbb{E}[\alpha_4(X_1, X_2)\alpha_1(X_2)] - m^{-2}\mathbb{E}[\alpha_1(X_1)\alpha_3(X_1)] \right. \\ &\quad \left. + n^{-2}\mathbb{E}[\beta_1(Y_1)\beta_3(Y_1)] + n^{-2}\mathbb{E}[\beta_4(Y_1; Y_2)\beta_1(Y_2)] \right\}, \\ Q_{m,n,\rho_A,\rho_B;2} &:= \sigma_{m,n}^{-3} \left\{ m^{-2}(\mathbb{E}[\alpha_1^3(X_1)/6 \right. \\ &\quad \left. + \alpha_1(X_1)\alpha_1(X_2)\alpha_2(X_1, X_2)] - n^{-2}(\mathbb{E}[\beta_1^3(Y_1)/6 + \beta_1(Y_1)\beta_1(Y_2)\beta_2(Y_1, Y_2)]) \right\} \\ &\quad + \frac{1}{2}\sigma_{m,n}^{-5} \left\{ (-m^{-3}\xi_{\alpha;1}^2 - m^{-2}n^{-1}\xi_{\beta;1}^2) \cdot \mathbb{E}[\alpha_1(X_1)\alpha_3(X_1) + \alpha_4(X_1; X_2)\alpha_1(X_2)] \right. \\ &\quad \left. + (m^{-1}n^{-2}\xi_{\alpha;1}^2 + n^{-3}\xi_{\beta;1}^2) \cdot \mathbb{E}[\beta_1(Y_1)\beta_3(Y_1) + \beta_4(Y_1; Y_2)\beta_1(Y_2)] \right\}, \end{aligned}$$

where $\xi_{\alpha;1}^2 := \text{Var}(\alpha_1(X_1))$ and $\xi_{\beta;1}^2 := \text{Var}(\beta_1(Y_1))$. Note that α_0 to α_4 , β_0 to β_4 are all $\asymp 1$ or $\asymp_p 1$ and $\sigma_{m,n}^2 \asymp m^{-1} + n^{-1}$, therefore, all of \mathcal{I}_0 , $Q_{m,n,\rho_A,\rho_B;1}$ and $Q_{m,n,\rho_A,\rho_B;2}$ are $\asymp (m \wedge n)^{-1/2}$. Due to space limit, the estimators of $\sigma_{m,n}^2$, α_0 , β_0 , $\mathbb{E}[\alpha_4(X_1, X_2)\alpha_1(X_2)]$ and so on are relegated to Section S.1 in Supplementary Material. These estimators lead to estimators $\widehat{\mathcal{I}}_0$, $\widehat{Q}_{m,n,\rho_A,\rho_B;1}$ and $\widehat{Q}_{m,n,\rho_A,\rho_B;2}$. It is noteworthy that all these quantities are computed independently using only A or B , and no information needs to be shared between two networks. Call R acyclic if it is a tree; otherwise call it cyclic. Define

$$\mathcal{M}_A = \mathcal{M}_A(\rho_A, m; R) := \begin{cases} (\rho_A \cdot m)^{-1} \cdot \log^{1/2} m + m^{-1} \cdot \log^{3/2} m, & \text{For acyclic } R, \\ \rho_A^{-r/2} \cdot m^{-1} \cdot \log^{1/2} m + m^{-1} \cdot \log^{3/2} m, & \text{For cyclic } R, \end{cases} \quad (5)$$

and define \mathcal{M}_B similarly. We now present our main theorem.

Theorem 1 (Population and empirical Edgeworth expansions). *Assume:*

1. *Network sizes satisfy:* $\log(m \vee n)/(m \wedge n) \rightarrow 0$;
2. *Either $\rho_A = O(\log m)^{-1}$ and $\rho_B = O(\log n)^{-1}$; or Cramer's condition holds for both networks:* $\limsup_{t \rightarrow \infty} |\mathbb{E}[e^{itg_{A;1}(X_1)}/\xi_{A;1}]| < 1$ and $\limsup_{t \rightarrow \infty} |\mathbb{E}[e^{itg_{B;1}(Y_1)}/\xi_{B;1}]| < 1$;

3. *Network sparsities satisfy: $\rho_A = \omega(m^{-1})$ and $\rho_B = \omega(n^{-1})$ if R is acyclic; and $\rho_A = \omega(m^{-1/r})$ and $\rho_B = \omega(n^{-1/r})$ if R is cyclic.*

Define the population Edgeworth expansion for $\widehat{T}_{m,n}$ as follows

$$G_{m,n}(u) := \Phi(u) - \varphi(u) \cdot \{Q_{m,n,\rho_A,\rho_B;1} + Q_{m,n,\rho_A,\rho_B;2} (u^2 - 1) + \mathcal{I}_0\},$$

and define the empirical Edgeworth expansion (EEE) $\widehat{G}_{m,n}(u)$ by replacing \mathcal{I}_0 , $Q_{m,n,\rho_A,\rho_B;1}$ and $Q_{m,n,\rho_A,\rho_B;2}$ by their estimators defined earlier. We have

$$\|F_{\widehat{T}_{m,n}}(u) - G_{m,n}(u)\|_\infty = O\left((m \wedge n)(m^{-1}\mathcal{M}_A + n^{-1}\mathcal{M}_B)\right), \quad (6)$$

$$\mathbb{P}\left\{\|F_{\widehat{T}_{m,n}}(u) - \widehat{G}_{m,n}(u)\|_\infty \geq (m \wedge n)(m^{-1}\mathcal{M}_A + n^{-1}\mathcal{M}_B)\right\} = O(m^{-1} + n^{-1}). \quad (7)$$

To our best knowledge, Theorem 1 addresses a much wider range of (m, n, ρ_A, ρ_B) than all existing similar works. For example, Ghoshdastidar et al. (2017) assumes $\rho_A, \rho_B \asymp 1$; and Agterberg et al. (2020) makes the restrictive assumption that $m/n \rightarrow \text{constant}$ for dense networks or $\rho_A m / (\rho_B n) \rightarrow \text{constant}$ for sparse networks. Moreover, under the same parameter configuration assumptions, our method achieves much stronger results. For instance, under the settings of Ghoshdastidar et al. (2017), our eq. (7) gives a higher-order accurate $O((m \wedge n)^{-1})$ distribution approximation error bound; to our best knowledge, this is the first result of its kind. Note that eq. (6) also implies the canonical Berry-Essen bound $\|F_{\widehat{T}_{m,n}}(u) - \Phi(u)\|_\infty = O((m \wedge n)^{-1/2})$ under appropriate network sparsity conditions. Also, compared to other approaches to improve risk control accuracy such as iterative bootstrap (Hall and Martin, 1988; Beran, 1987, 1988), which though has not yet been formulated for the network setting, our empirical Edgeworth expansion method computes much faster and has a much better provable error bound.

3.3 Two-sample test and Cornish-Fisher confidence interval

We now present our approach to two-sided test. Parallel results for one-sided alternatives can be easily derived.

$$H_0 : d_{m,n,\rho_A,\rho_B} = 0, \quad \text{vs} \quad H_a : d_{m,n,\rho_A,\rho_B} \neq 0. \quad (8)$$

The empirical p-value produced by our method is $2 \cdot \min\{\widehat{G}_{m,n}(\widehat{T}_{m,n}^{(\text{obs})}), 1 - \widehat{G}_{m,n}(\widehat{T}_{m,n}^{(\text{obs})})\}$, where we define $\widehat{T}_{m,n}^{(\text{obs})} := \widehat{D}_{m,n} / \widehat{S}_{m,n}$. We also formulate the Cornish-Fisher confidence interval by inverting the Edgeworth expansion. Define $q_{\widehat{T}_{m,n};\alpha} := \arg \min_{q \in \mathbb{R}} \{F_{\widehat{T}_{m,n}}(q) \geq \alpha\}$ to be the true lower- α quantile of the distribution of $\widehat{T}_{m,n}$. We can approximate $q_{\widehat{T}_{m,n};\alpha}$ by $\widehat{q}_{\widehat{T}_{m,n};\alpha} := z_\alpha + \widehat{\mathcal{I}}_0 + \widehat{Q}_{m,n,\rho_A,\rho_B;1} + \widehat{Q}_{m,n,\rho_A,\rho_B;2}(z_\alpha^2 - 1)$ where $z_\alpha := \Phi^{-1}(\alpha)$. The two-sided Cornish-Fisher CI for estimating d_{m,n,ρ_A,ρ_B} is

$$\left(\widehat{D}_{m,n} - \widehat{q}_{\widehat{T}_{m,n};1-\alpha/2} \cdot \widehat{S}_{m,n}, \widehat{D}_{m,n} - \widehat{q}_{\widehat{T}_{m,n};\alpha/2} \cdot \widehat{S}_{m,n}\right). \quad (9)$$

The higher-order accuracy of our distribution approximation leads to accurate controls of type-I error in the hypothesis test and the confidence level associated with the confidence interval.

Theorem 2. *Under the conditions of Theorem 1, we have*

1. *The type I error of the test (8) with nominal level α has an actual type I error probability of $\alpha + O((m \wedge n)(m^{-1}\mathcal{M}_A + n^{-1}\mathcal{M}_B))$. The type II error of the test (8) is $o(1)$ when the true separation satisfies $d_{m,n,\rho_A,\rho_B} = \omega(m^{-1/2} + n^{-1/2})$.*
2. *The Cornish-Fisher confidence interval (9) with nominal confidence level $1 - \alpha$ has an actual coverage probability of $1 - \alpha + O((m \wedge n)(m^{-1}\mathcal{M}_A + n^{-1}\mathcal{M}_B))$. The length of the confidence interval is $O(m^{-1} + n^{-1})$.*

The next theorem shows that our method, while enjoying higher-order accurate risk controls, simultaneously achieves minimax optimality.

Theorem 3. 1. *(Rate-optimality of the separation condition of our test) For any fixed $\alpha \in (0, 1)$, there exists population models:*

- * *Under H_0 : network 1 $\sim \rho_A \cdot f_0(u, v)$, network 2 $\sim \rho_B \cdot f_0(u, v)$;*
- * *Under H_a : network 1 $\sim \rho_A \cdot f_0(u, v)$, network 2 $\sim \rho_B \cdot f_b(u, v)$*

for some $\rho_A, \rho_B, f_0, f_a, f_b$, such that $d_{m,n,\rho_A,\rho_B} = O(m^{-1/2} + n^{-1/2})$ under H_a , while any procedure \mathcal{T} for the hypothesis test (8) suffers

$$\mathbb{P}_{\mathcal{T}}(\text{Reject } H_0 | H_0) + \mathbb{P}_{\mathcal{T}}(\text{Keep } H_0 | H_a) \geq C > 0 \quad (10)$$

for some constant $C > 0$ as $m, n \rightarrow \infty$.

2. *(Rate-optimality of the expected length of our confidence interval) For any fixed $\alpha \in (0, 1)$,*

$$\min_{\mathcal{I}: \mathbb{P}(d_{m,n,\rho_A,\rho_B} \in \mathcal{I}) \rightarrow 1 - \alpha} \max_{\rho_A, \rho_B, f_a, f_b} \mathbb{E}[|\mathcal{I}|] \geq C(m^{-1/2} + n^{-1/2}) \quad (11)$$

for some constant $C > 0$.

Remark 1. *By Theorem 2 and Theorem 3, respectively, our method enjoys both higher-order accurate risk control and power-optimality. Importantly, we emphasize that achieving either of these two desirable properties is not difficult. For instance, a simple normal approximation also enjoys the optimality properties in Theorem 3, but not that in Theorem 2. However, achieving both higher-order accurate risk control and power-optimality, is challenging. To our best knowledge, our method is the first to provably achieve both.*

4 Network hashing: offline database maintenance and fast querying

Suppose we query a graph $A \in \{0, 1\}^{m \times m}$ in a graph database that contains K network entries $\{B_k\}_{k=1, \dots, K}$ of sizes n_1, \dots, n_K and sparsity parameters $\rho_{B_1}, \dots, \rho_{B_K}$, where any or all of

m, K, n_1, \dots, n_K could potentially be very large. Our method effectively addresses this challenge by hashing database entries with offline computation into just a few summary statistics. When querying a keyword A , we only need to compare the hash of A to entries’ hashes. This provides a very fast screening algorithm to quickly narrow down the search range. Our hashing-query procedure also protects data privacy, since all parties only need to disclose network summary statistics, not the entire networks. The fast speed and enhanced privacy may cater to the urgent needs of multi-institutional clinical research collaboration on Alzheimer (Chen et al., 2022c) and other diseases, where privacy protection and high communication cost are two paramount concerns when sharing sensitive patient-level data (Chen et al., 2022a). Using our method, researchers can conveniently build, maintain and query a large similarity graph between patient brain images across multiple hospitals for disease subtyping with improved privacy protection and high communication efficiency. We do clarify that mathematical quantification of privacy protection would be an interesting future work but not the purpose of this paper.

Algorithm 1 Network hashing

Input: Network database: $\{B_1, \dots, B_K\}$

Output: Each B_k hashes into a short vector of its own summary statistics

Step: For $k = 1, \dots, K$ and for all $i^{(k)} = 1, \dots, n_k$ and $1 \leq \{i_1^{(k)} \neq i_2^{(k)}\} \leq n_k$ and for each motif name, compute and output $\hat{\rho}_B, \hat{V}_n, \hat{g}_{B;1}(Y_{i^{(k)}}), \hat{g}_{B;2}(Y_{i_1^{(k)}}, Y_{i_2^{(k)}}), \hat{g}_{\rho_B;1}(Y_{i^{(k)}}), \hat{g}_{\rho_B;2}(Y_{i_1^{(k)}}, Y_{i_2^{(k)}})$ by eq. (S11)-(S14) in Section S.1 of Supplementary Material, and also output the motif name and m .

Algorithm 2 Fast querying

Input: Queried “keyword” network A ; Hashed database (output of Algorithm 1); level α

Output: A list of B_k ’s with similar network moments to A ; or “not found” (empty query result)

Steps:

1. Compute $\hat{\rho}_A, \hat{U}_m, \hat{g}_{A;1}(X_i), \hat{g}_{A;2}(X_{i_1}, X_{i_2}), \hat{g}_{\rho_A;1}(X_i), \hat{g}_{\rho_A;2}(X_{i_1}, X_{i_2})$ by eq. (S11)-(S14) in Section S.1 of Supplementary Material using A .
2. For $k = 1, \dots, K$, for network pair (A, B_k) , compute

$$\hat{p}_k := 2 \min \left\{ \hat{G}_{m, n_k}(\hat{T}_{m, n_k}^{(\text{obs})}), 1 - \hat{G}_{m, n_k}(\hat{T}_{m, n_k}^{(\text{obs})}) \right\} \quad (12)$$

using statistics computed by Algorithm 1 and Step 1 of Algorithm 2

3. Extract entries satisfying $\{B_k : \hat{p}_k \geq \alpha\}$ as candidates passing our screening algorithm, whose match with the queried entry is to be further inspected.
-

Algorithms 1 and 2 show the offline nature of our hashing procedure, which can prepare database entries for fast query without knowing the queried keyword. This is very different from most existing methods such as Ghoshdastidar et al. (2017); Tang et al. (2017); Agterberg et al. (2020), which do not have a hashing stage and their query methods unavoidably require at least

$\Omega(mn_k)$ cross-computation, where m is the size of the queried keyword network. The hashing cost on each individual entry is $O(\rho_n^{r-1} \cdot n^r)$, see Section III.A of Ahmed et al. (2015). To see the distinction in computational cost, suppose all entries have same sizes $n_1 = \dots = n_K = n$ and density levels $\rho_{B_1} = \dots = \rho_{B_K} = \rho_B$ and there are K_q incoming queries. Then our method costs $O(K\rho_B^{r-1}n^r + KK_q)$. In sharp contrast, existing methods that requires cross-computation cost $O(KK_qmn)$, which will soon burn out the query system as K_q becomes very large.

Next, we give a finite-sample error bound for type I and type II query errors.

Theorem 4. *Under the conditions of Theorem 1, there exist positive constants $C_1, C_2, C_3, C_4 > 0$, such that for some $\delta := \delta_{m, n_k} := C_1(m^{-1/2} \log m + n_k^{-1/2} \log n_k)$, setting $\mathcal{K}_{d, \delta} := \{k \in \{1, \dots, K\}, |d_{m, n_k, \rho_A, \rho_{B_k}}^{(k)}| \geq \delta_{m, n_k}\}$, the query result produced by Algorithms 1 and 2 satisfy*

$$\begin{aligned} \text{(Type I error)} \quad & \sum_{k \in [1:K] \setminus \mathcal{K}_{d, \delta}} \mathbb{P}(\hat{p}_k < \alpha) = \sum_{k \in [1:K] \setminus \mathcal{K}_{d, \delta}} \left(\alpha + O(m^{-1/2} \log m + n_k^{-1/2} \log n_k) \right). \\ \text{(Type II error)} \quad & \sum_{k \in \mathcal{K}_{d, \delta}} \mathbb{P}(\hat{p}_k \geq \alpha) = \sum_{k \in \mathcal{K}_{d, \delta}} O(m^{-C_3} + n_k^{-C_3}), \end{aligned}$$

5 Simulations and data examples

5.1 Simulation 1: distribution approximation error

Our first simulation aims to illustrate our method's higher-order accuracy in approximating the distribution of $\hat{T}_{m, n}$. We generate data from the two graphons $f_A(u, v) = 1.71 \cdot (u+v)^2/2$ and $f_B(u, v) = 1.38 \cdot \exp\{-(u+v)/3\}$, and approximately the true $F_{\hat{T}_{m, n}}(u)$ by $n_{\text{MC}} := 10^5$ Monte Carlo replications. Accuracy is measured by the truncated Kolmogorov distance $\sup_{u \in [-2, 2]} |\hat{F}_{\hat{T}_{m, n}}(u) - F_{\hat{T}_{m, n}}(u)|$. We compare to three benchmark methods: $N(0, 1)$ approximation, node subsampling, and node resampling. Here, the node subsampling and resampling methods are in our own formulation, which extend Bhattacharyya and Bickel (2015) and Green and Shalizi (2022), respectively. The algorithm is given in Algorithm 3. We set $m_{\text{sub}} = m^{1/2}$, $n_{\text{sub}} = n^{1/2}$; and set $N_{\text{boot}} = 200$ for both subsampling and resampling. Taking subsampling as an example, a key distinction between our

Algorithm 3 Node subsampling/resampling bootstrap for two-sample inference

Input: Networks A, B ; bootstrap repetition N_{boot} ; if subsampling: subsample sizes $m_{\text{sub}}, n_{\text{sub}}$

Output: Bootstrapped studentized empirical moment discrepancies $\{\hat{T}_{m, n}^{(b)}\}_{b=1, \dots, N_{\text{boot}}}$

Steps: For $b = 1, \dots, N_{\text{boot}}$, do

1. Node subsample/resample A, B , obtain $A^{(b)}, B^{(b)}$. If resampling, randomly sample m nodes \mathcal{J}_A from $[1 : m]$ with replacement; if subsampling, randomly sample m_{sub} nodes \mathcal{J}_A from $[1 : m]$ without replacement; In either case, set $A^{(b)} \leftarrow A_{\mathcal{J}_A}$; do the same for B
 2. Compute $\hat{T}_{m, n}^{(b)}$ using (3) and (4), with $A^{(b)}, B^{(b)}$ as the input
-

subsampling and Bhattacharyya and Bickel (2015); Lunde and Sarkar (2019) is that we bootstrap the studentization $\hat{T}_{m,n}$ that we formulate in (3) and (4), whereas they bootstrap the unstudentized $\hat{D}_{m,n}$ or its standardization. As pointed out by Wasserman (2006); Hall (2013), studentization is the key to achieve higher-order accuracy, which standardization does not achieve. Ghoshdastidar et al. (2017) uses a conservative variance estimate, which leads to their test statistic that is not a studentized. Their test method is based on the convergence of their test statistic, without characterizing the statistic’s distribution, thus is not comparable. To ease visualization, in this simulation, we set $m = n \in \{10, 20, 40, 80, 160\}$. We did not test on larger networks because node resampling bootstrap costs more than 12 hours for $n = 320$.

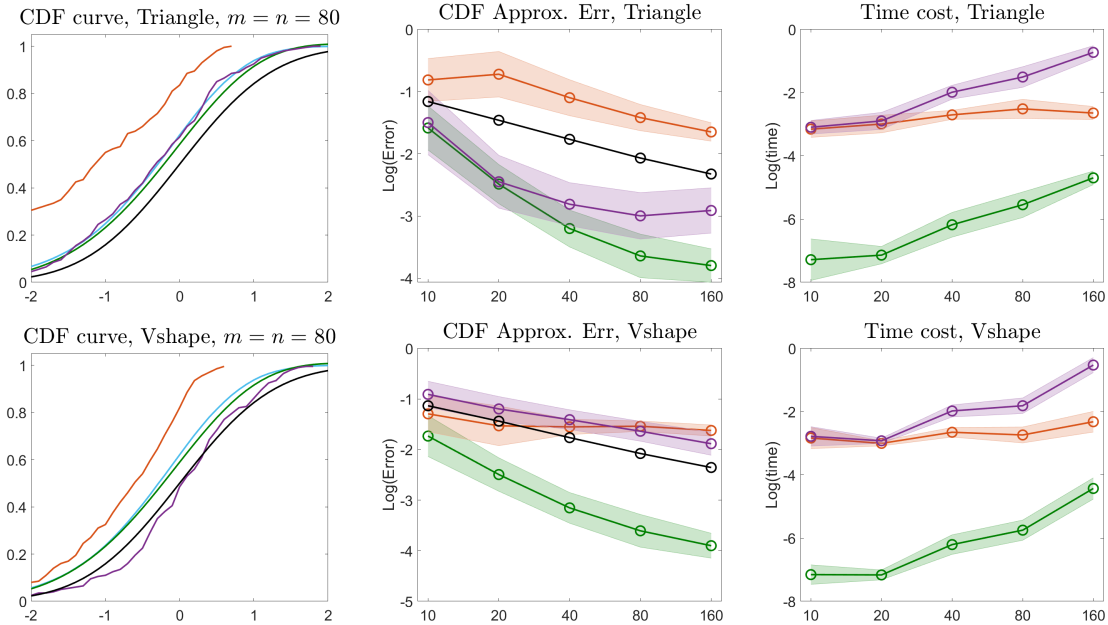


Figure 1: Distribution approximation accuracy comparison. Left: true and estimated cumulative distribution functions; middle: comparison of logarithm Kolmogorov-distance; right: logarithm computation time, notice $N(0, 1)$ costs no time to approximate $F_{\hat{T}_{m,n}}$. Cyan is the Monte Carlo evaluation of the true $F_{\hat{T}_{m,n}}$; green is our method; black is $N(0, 1)$; and orange and purple are node subsampling and resampling, respectively, formulated by our Algorithm 3.

Figure 1 shows the result. The vertical error bar shows the standard deviation of our method over 100 repeated experiments. The result echoes our method’s higher-order accuracy that improves over $N(0, 1)$ due to bias correction. It also confirms our method’s computational efficiency.

5.2 Simulation 2: Coverage probability of Cornish-Fisher confidence interval

As recognized by classical literature Hall (2013); Beran (1987), one main merit of higher-order accurate CDF approximation is that it enables higher-order accurate control of the confidence

interval’s actual coverage probability. In this experiment, we evaluate the discrepancy between the actual coverage probability and nominal confidence level as the performance measure. We inherit the set up of Simulation 1, set $1 - \alpha = 90\%$, but experiment on more (m, n) combinations $(m, n) \in \{10, 20, 40, 80, 160\}^2$. We compare to the same benchmarks in Simulation 1.

Figure 2 shows that our method controls coverage probabilities more accurately around the nominal level $1 - \alpha$ in most settings, except in the case where one network has only $m = 10$ nodes. This is not surprising since the remainder terms ignored in the analytical approximation may be no longer ignorable when the network is very small. We recall that both node bootstrap methods in this simulation are also devised based on our formulation of $\hat{T}_{m,n}$. Node resampling shows good accuracy and robustness on some small network examples, but it is not scalable: it takes more than 12 hours to run node resampling experiments for $m \vee n = 320$ settings. Due to page limit, we sink the numerical result tables to Section S.2.1 in Supplementary Material.

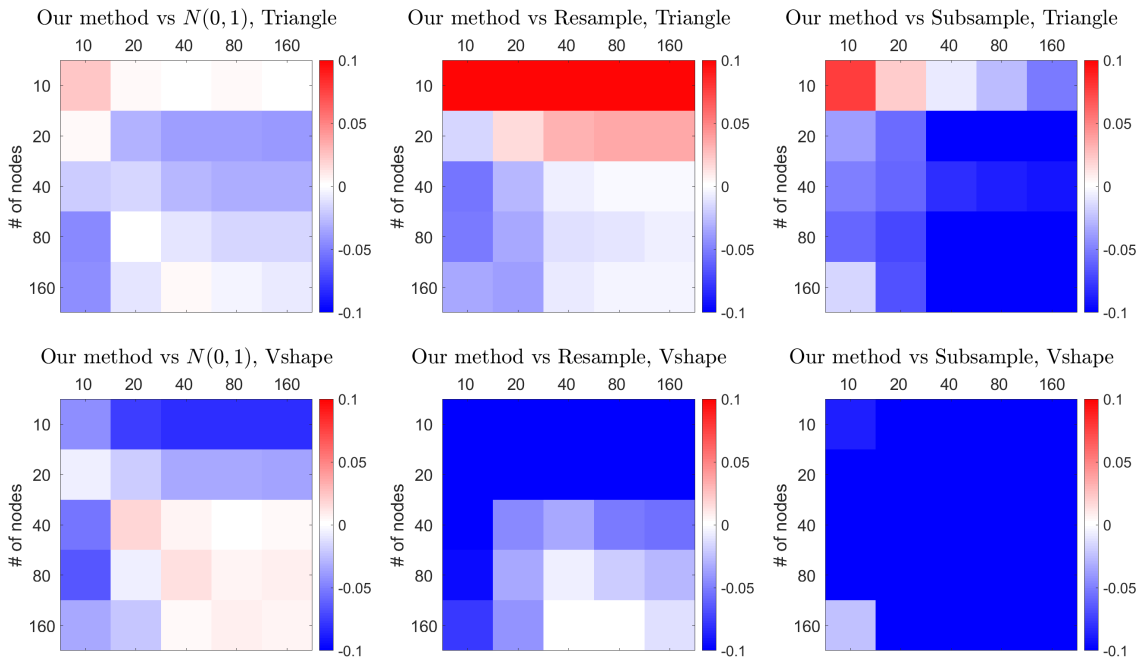


Figure 2: Comparison of CI coverage accuracy. Bluer pixel indicates more advantage of our method over the compared method. Here we only show accuracy comparisons; evidence of marginal accuracy of our method in Section S.2.1 in Supplementary Material.

5.3 Simulation 3: Network hashing and querying

In this experiment, we simulate a large network database consisting of 10 different graphon models, each corresponds to 100 adjacency matrices as database entries. We use our Algorithm 1 to hash database entries, and then evaluate the accuracy of our Algorithm 2 on querying two representative keyword networks. We compare the time costs of hashing and querying with 30 repeated experiments. To save memory, in each experiment we only re-generate the queried

keyword network but reuse the database generated by the first repetition. We conduct two sub-simulations. Sub-simulation 1 aims to compare different methods’ AUC curves and time costs, therefore, we generate one keyword network from one of the constituent graphons in the database. Sub-simulation 2 aims to visualize a sketch of our method’s query results, therefore, we compare the query results of two different keyword networks from graphons inside and outside the database, respectively. Due to page limit, we sink the formulation of database graphons and the two keyword networks to Section S.2.1 in Supplementary Material. When querying, we perform steps 1 & 2 of Algorithm 2 to evaluate the ROC curves and AUC scores that measure the accuracy of our method in ranking database entries by similarity to the queried keyword network. Due to page limit, we only compare AUC scores for all methods. For simplicity, we equate all network sizes: $m = n_1 = \dots = n_K \in \{100, 200, 400, 800, 1600\}$. In this simulation, we compare our method to three more benchmarks: NetLSD (Tsitsulin et al., 2018), NetComp (Wills and Meyer, 2020) and NonparGraphTesting (Agterberg et al., 2020). These methods are not moment-based so they are inapplicable for comparison in Simulations 1 and 2. We repeat each experiment 30 times and cap the total running time for each method for each network size at 12 hours.

Row 1 of Figure 3 shows the result for sub-simulation 1. The ROC and AUC plots confirm our Algorithm 2’s high accuracy in screening database entries similar to the queried keyword. The time cost plot clearly shows the speed advantage of our method. Importantly, to query a new keyword, our method only costs the time described by the pink curve tagged query time, and we would not need to repeat the hashing step; in stark contrast, all the other methods would need to rerun, which incurs the same time costs shown on their curves. This experiment therefore demonstrate our method’s significant advantage in scalability. Row 2 of Figure 3 shows the result for sub-simulation 2 by comparing the p-value distributions associated with both keywords. We marked the typically used 5% significance line in dashed blue. Red bars to the right of it are making type I error. As n increases, we see the expected result that all red bars move to the left of the dashed blue threshold line. But the cyan bars, which corresponds to power, should be interpreted with much more carefulness. Notice that by construction, the keyword network corresponding to cyan bars only matches 10% database entries but does not match the remaining 90%, so the majority chunk of cyan bars should still remain distant from 0 as n increases, see also the full-X-scale plots in Section S.2.2 in Supplementary Material.

5.4 Data example 1: Google+ ego-network data

In this example, we study the well-known SNAP-Gplus data set (Leskovec and Mcauley, 2012). It consists of 132 ego-networks in severely varying sizes and densities. The combined network consists of more than 100 thousand nodes and 1.36 million edges. Existing works on this data set typically analyze the 132 ego-networks separately from each other (Leskovec and Mcauley, 2012; Yang et al., 2013); while we are interested in exploring the structural similarity relationships between these ego-networks. We pre-process the data by symmetrizing the ego-networks, eliminating 2 ego-networks with ≤ 10 nodes. Our two-sample inference method then produces a similarity graph between the remaining 130 ego-nodes. Table 1 row 1 reports the time costs of all methods. It turns out that subsampling is the only benchmark that can finish running. We use empirical p-values to measure network similarity.

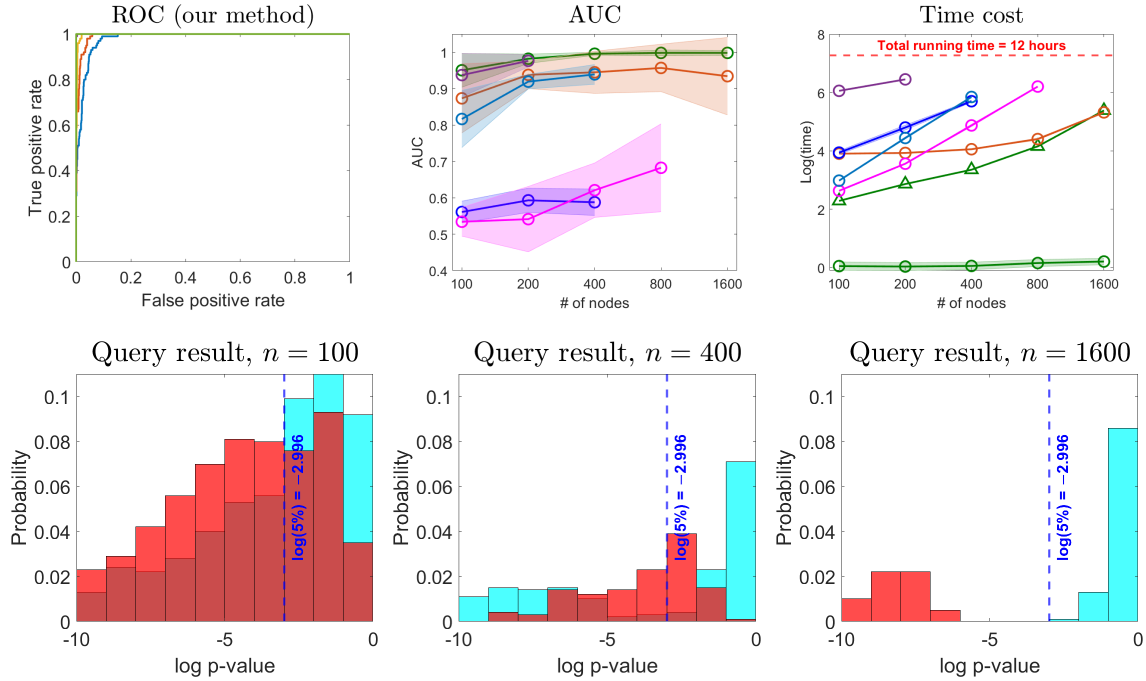


Figure 3: Database offline hashing and querying. Row 1: comparison of methods on query accuracy and time cost. In row 1, plot 1, blue, orange, yellow, violet and green curves correspond to the common network size $n \in \{100, 200, 400, 800, 1600\}$, respectively; In row 1, plots 2 and 3, our method, subsampling and resampling inherit the color schemes from Figure 1, where in plot 3, triangle-marked green curve is our method’s hashing time, circle-marked is query time; deep blue is NonparGT, magenta is NetLSD and light blue is NetComp. Row 2: histograms of logarithm p-values produced by our method, comparing database entries to a keyword generated by a graphon: 1. inside the database, bars in cyan; and 2. outside the database, bars in red. We only plot for X-axis range $[-10, 0]$; full plots in Section S.2.2 in Supplementary Material. We note that in Row 2, Plot 2, keeping the X-axis range consistent with $n = 100, 400$ plots would cut out many cyan bars on the far left.

Figure 4 reports the result. In the left panel, our method identifies 3 loosely clustered subgroups among ego-networks with further internal structures. To further improve presentation, we post-process the 130×130 similarity graph by reordering nodes based on the estimated graphon slice similarity measure (Zhang et al., 2017). We find this sorting method to be more effective when the similarity graph displays within-group heterogeneity. Compared to our method, the p-values estimated by node subsampling seem to be systemically lower than our method. To intuitively understand why network subsampling may inflate type I error in finite-sample examples, consider two moderately large networks generated from the same model, but the model has much heterogeneity. Consequently, there is a good chance that subsampling may sample different parts of the two networks and incorrectly reject the null hypothesis.

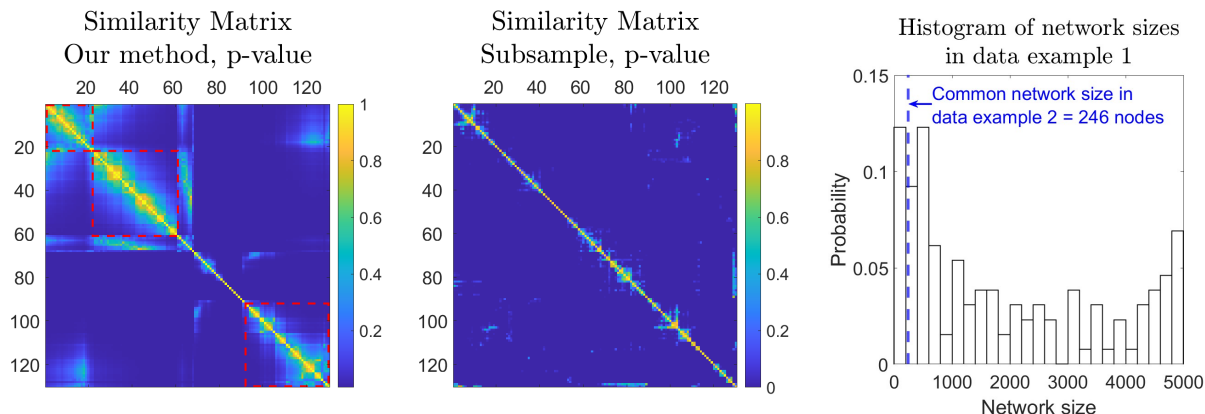


Figure 4: Data example 1: Google+ ego-networks. Similarity graphs by our method on the left, and subsampling in the middle. In both plots, nodes were reordered using graphon slice similarity (Zhang et al., 2017). The right panel illustrates the distribution of ego-network sizes.

Table 1: Time cost comparison table. Unit is second. Timeout is 12 hours = 43200 seconds.

	Our method (hash)	Our method (test)	Subsample	Resample
Data example 1	135.76	19.80	10888.00	(Timeout)
Data example 2	3.01	60.74	2547.51	(Timeout)
	NonparGT	NetLSD	NetComp	
Data example 1	(Numerical error)	(Timeout)	(Timeout)	
Data example 2	4327.09	(Numerical error)	4304.51	

5.5 Data example 2: Brain connectome data for schizophrenia research

This data set, collected by Adhikari et al. (2019), consists of functional brain connectivity networks among 103 patients with schizophrenia and 124 healthy people as normal controls. We follow the protocol by Adhikari et al. (2019) to pre-process the resting-state fMRI data. All individuals' networks share a common set of 246 nodes that represent different regions of interests. Each edge

is a Fisher Z-transformed correlation between the blood-oxygen-level-dependent signals at the two terminal nodes. We test all methods for pairwise comparison and use the technique similar to data example 1 to reorder nodes in the obtained similarity graph to facilitate result interpretation.

Figure 5 shows the result. Our method identified several subgroups that are potentially subtypes of the disease worth further investigation. The result significantly enriches over many network two-sample test methods in existing literature (Yuan and Wen, 2021; Bravo-Hermsdorff et al., 2021; Chen et al., 2022b), which only produce a binary decision of whether the two groups of networks are structurally identical but could not discover within-group structures like our method provides. Row 2 of Figure 5 suggests that among females, subgroups SZ2, SZ3 and NC2 mostly consist of mid-age to seniors, whereas NC1 is particularly young; among males, SZ4b, NC1 and NC3 exhibit different levels of concentration around their own particular age groups. Moreover, the similarity graph produced by our method finds structural similarities between some patient-normal subgroup pairs, such as (SZ1, NC2) and (SZ2, NC3). Therefore, it might be of interest for biomedical researchers to further compare these subgroup pairs and look for disease-linked differences. Similar to data example 1, here, subsampling also identifies much less similarities between individual pairs. NonparGT identifies even less pairwise similarity, understandably since its null hypothesis requires the two network models to be completely identical. NetComp does not produce an empirical p-value but an estimated distance between each network pair. Its output a similarity graph with patterns different from ours and of independent interest. Row 2 of Table 1 records running time. Our method again shows significant speed advantage by only computing the hashing once for each network, and all pair-wise comparisons can be done in $O(1)$ time. To understand why our method spends much less time in hashing but more time in pairwise comparisons in data example 2 than that in data example 1, we refer to the network size histogram in Figure 4. Most network sizes in data example 1 are in thousands, much larger than the common network size of 246 nodes in data example 2; while data example 2 contains 75% more networks than data example 1, and $1.75^2 \approx 3$ explains the inflation of pairwise comparison time.

Supplementary Material

The Supplementary Material contains the following contents: 1. definitions of the α - and β -terms in Section 3.2 and their estimators 2. additional simulation results.

References

- Abbe, E. (2017). Community detection and stochastic block models: recent developments. *The Journal of Machine Learning Research*, 18(1):6446–6531.
- Adhikari, B. M., Hong, L. E., Sampath, H., Chiappelli, J., Jahanshad, N., Thompson, P. M., Rowland, L. M., Calhoun, V. D., Du, X., and Chen, S. (2019). Functional network connectivity impairments and core cognitive deficits in schizophrenia. *Human brain mapping*, 40(16):4593–4605.

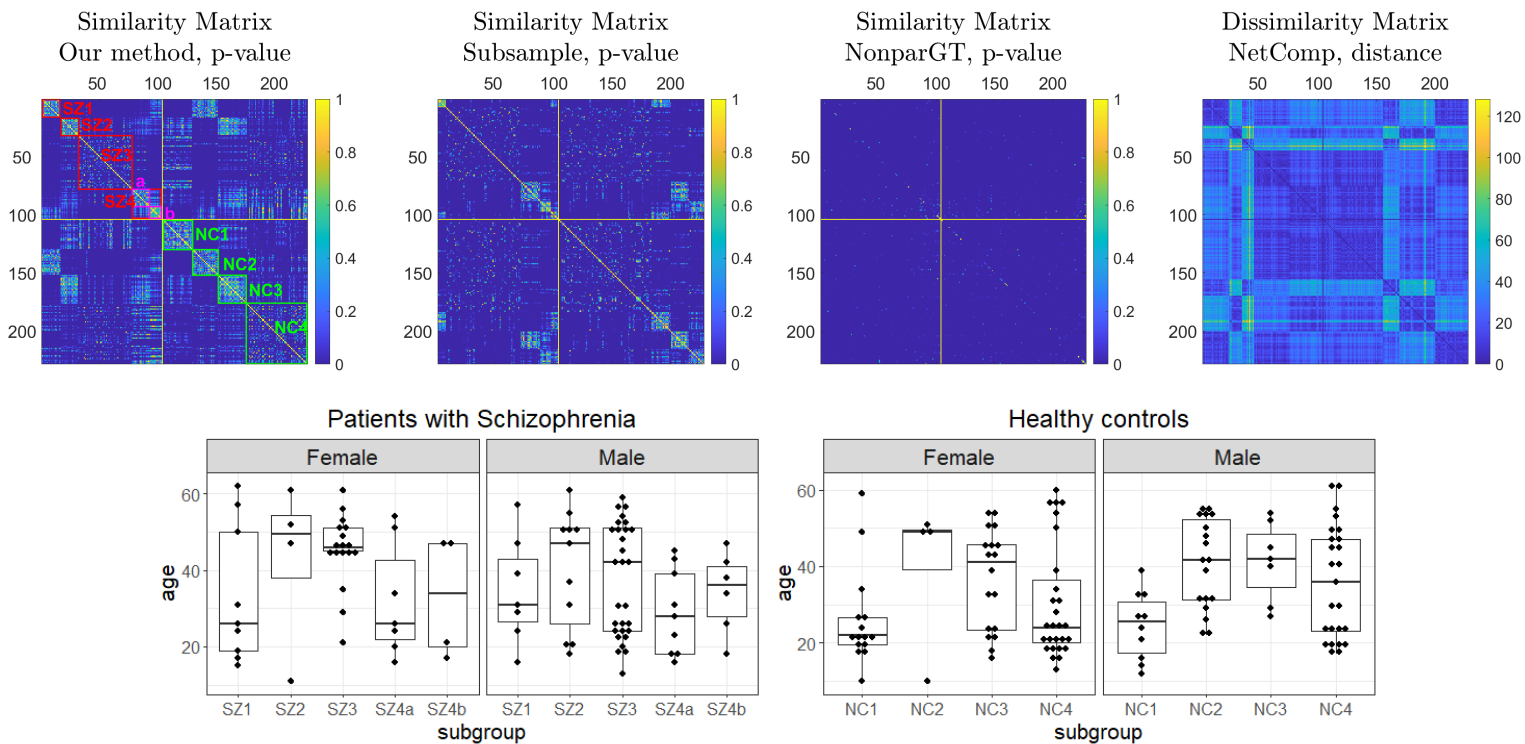


Figure 5: Data example 2: schizophrenia. Row 1: similarity graph between brain images, constructed by our method using p-values. Nodes 1–103 are patients and nodes 104–227 are healthy people. We added artificial yellow lines to separate the two groups. Row 2: age distributions in each subgroup identified by our method for female and male participants.

- Agterberg, J., Tang, M., and Priebe, C. (2020). Nonparametric two-sample hypothesis testing for random graphs with negative and repeated eigenvalues. *arXiv preprint arXiv:2012.09828*.
- Ahmed, N. K., Neville, J., Rossi, R. A., and Duffield, N. (2015). Efficient graphlet counting for large networks. In *2015 IEEE International Conference on Data Mining*, pages 1–10. IEEE.
- Arroyo, J., Sussman, D. L., Priebe, C. E., and Lyzinski, V. (2021). Maximum likelihood estimation and graph matching in errorfully observed networks. *Journal of Computational and Graphical Statistics*, 30(4):1111–1123.
- Banerjee, D. and Ma, Z. (2017). Optimal hypothesis testing for stochastic block models with growing degrees. *arXiv preprint arXiv:1705.05305*.
- Beran, R. (1987). Prepivoting to reduce level error of confidence sets. *Biometrika*, 74(3):457–468.
- Beran, R. (1988). Prepivoting test statistics: a bootstrap view of asymptotic refinements. *Journal of the American Statistical Association*, 83(403):687–697.
- Bhattacharya, B. B., Das, S., and Mukherjee, S. (2022). Motif estimation via subgraph sampling: The fourth-moment phenomenon. *The Annals of Statistics*, 50(2):987–1011.
- Bhattacharyya, S. and Bickel, P. J. (2015). Subsampling bootstrap of count features of networks. *The Annals of Statistics*, 43(6):2384–2411.
- Bickel, P. J. and Chen, A. (2009). A nonparametric view of network models and newman–girvan modularities. *Proceedings of the National Academy of Sciences*, 106(50):21068–21073.
- Bickel, P. J., Chen, A., and Levina, E. (2011). The method of moments and degree distributions for network models. *The Annals of Statistics*, 39(5):2280–2301.
- Borgs, C., Chayes, J., and Lovász, L. (2010). Moments of two-variable functions and the uniqueness of graph limits. *Geometric And Functional Analysis*, 19(6):1597–1619.
- Bravo-Hermsdorff, G., Gunderson, L. M., Maugis, P.-A., and Priebe, C. E. (2021). A principled (and practical) test for network comparison. *arXiv preprint arXiv:2107.11403*.
- Chen, A. A., Luo, C., Chen, Y., Shinohara, R. T., Shou, H., Initiative, A. D. N., et al. (2022a). Privacy-preserving harmonization via distributed combat. *Neuroimage*, 248:118822.
- Chen, L., Josephs, N., Lin, L., Zhou, J., and Kolaczyk, E. D. (2022+b). A spectral-based framework for hypothesis testing in populations of networks. *Statistica Sinica (In press)*.
- Chen, P., Yao, H., Tijms, B. M., Wang, P., Wang, D., Song, C., Yang, H., Zhang, Z., Zhao, K., Qu, Y., et al. (2022c). Four distinct subtypes of alzheimer’s disease based on resting-state connectivity biomarkers. *Biological Psychiatry*.
- Decelle, A., Krzakala, F., Moore, C., and Zdeborová, L. (2011). Inference and phase transitions in the detection of modules in sparse networks. *Physical Review Letters*, 107(6):065701.

- Gao, C. and Lafferty, J. (2017). Testing network structure using relations between small subgraph probabilities. *arXiv preprint arXiv:1704.06742*.
- Gao, C., Lu, Y., and Zhou, H. H. (2015). Rate-optimal graphon estimation. *The Annals of Statistics*, 43(6):2624–2652.
- Gao, C., Ma, Z., Zhang, A. Y., and Zhou, H. H. (2018). Community detection in degree-corrected block models. *Annals of Statistics*, 46(5):2153–2185.
- Ghoshdastidar, D., Gutzeit, M., Carpentier, A., and von Luxburg, U. (2017). Two-sample tests for large random graphs using network statistics. In *Conference on Learning Theory*, pages 954–977. PMLR.
- Ghoshdastidar, D., Gutzeit, M., Carpentier, A., and Von Luxburg, U. (2020). Two-sample hypothesis testing for inhomogeneous random graphs. *The Annals of Statistics*, 48(4):2208–2229.
- Ghoshdastidar, D. and Von Luxburg, U. (2018). Practical methods for graph two-sample testing. *Advances in Neural Information Processing Systems*, 31.
- Ginestet, C. E., Li, J., Balachandran, P., Rosenberg, S., and Kolaczyk, E. D. (2017). Hypothesis testing for network data in functional neuroimaging. *The Annals of Applied Statistics*, pages 725–750.
- Green, A. and Shalizi, C. R. (2022). Bootstrapping exchangeable random graphs. *Electronic Journal of Statistics*, 16(1):1058 – 1095.
- Hall, P. (2013). *The Bootstrap and Edgeworth Expansion*. Springer Science & Business Media.
- Hall, P. and Martin, M. A. (1988). On bootstrap resampling and iteration. *Biometrika*, 75(4):661–671.
- Hoeffding, W. (1948). A class of statistics with asymptotically normal distribution. *The Annals of Mathematical Statistics*, 19(3):293–325.
- Hunter, D. R., Handcock, M. S., Butts, C. T., Goodreau, S. M., and Morris, M. (2008). ergm: A package to fit, simulate and diagnose exponential-family models for networks. *Journal of Statistical Software*, 24(3).
- Jin, J., Ke, Z., and Luo, S. (2018). Network global testing by counting graphlets. In *International Conference on Machine Learning*, pages 2333–2341. PMLR.
- Kolaczyk, E. D., Lin, L., Rosenberg, S., Walters, J., and Xu, J. (2020). Averages of unlabeled networks: Geometric characterization and asymptotic behavior. *The Annals of Statistics*, 48(1):514–538.
- Leskovec, J. and Mcauley, J. (2012). Learning to discover social circles in ego networks. *Advances in Neural Information Processing Systems*, 25.

- Levin, K. and Levina, E. (2019). Bootstrapping networks with latent space structure. *arXiv preprint arXiv:1907.10821*.
- Li, Y. and Li, H. (2018). Two-sample test of community memberships of weighted stochastic block models. *arXiv preprint arXiv:1811.12593*.
- Lunde, R. and Sarkar, P. (2019). Subsampling sparse graphons under minimal assumptions. *arXiv preprint arXiv:1907.12528*.
- Lyzinski, V., Fishkind, D. E., Fiori, M., Vogelstein, J. T., Priebe, C. E., and Sapiro, G. (2015). Graph matching: Relax at your own risk. *IEEE Transactions on Pattern Analysis and Machine Intelligence*, 38(1):60–73.
- Maesono, Y. (1997). Edgeworth expansions of a studentized u-statistic and a jackknife estimator of variance. *Journal of Statistical Planning and Inference*, 61(1):61–84.
- Maugis, P.-A., Olhede, S., Priebe, C., and Wolfe, P. (2020). Testing for equivalence of network distribution using subgraph counts. *Journal of Computational and Graphical Statistics*, 29(3):455–465.
- Olhede, S. C. and Wolfe, P. J. (2014). Network histograms and universality of blockmodel approximation. *Proceedings of the National Academy of Sciences*, 111(41):14722–14727.
- Sabanayagam, M., Vankadara, L. C., and Ghoshdastidar, D. (2021). Graphon based clustering and testing of networks: Algorithms and theory. *arXiv preprint arXiv:2110.02722*.
- Tang, M., Athreya, A., Sussman, D. L., Lyzinski, V., Park, Y., and Priebe, C. E. (2017). A semiparametric two-sample hypothesis testing problem for random graphs. *Journal of Computational and Graphical Statistics*, 26(2):344–354.
- Tsitsulin, A., Mottin, D., Karras, P., Bronstein, A., and Müller, E. (2018). Netlsd: hearing the shape of a graph. In *Proceedings of the 24th ACM SIGKDD International Conference on Knowledge Discovery & Data Mining*, pages 2347–2356.
- Wasserman, L. (2006). *All of Nonparametric Statistics*. Springer Science & Business Media.
- Wills, P. and Meyer, F. G. (2020). Metrics for graph comparison: a practitioner’s guide. *Plos one*, 15(2):e0228728.
- Yang, J., Han, C., and Airolidi, E. (2014). Nonparametric estimation and testing of exchangeable graph models. In *Artificial Intelligence and Statistics*, pages 1060–1067. PMLR.
- Yang, J., McAuley, J., and Leskovec, J. (2013). Community detection in networks with node attributes. In *2013 IEEE 13th international conference on data mining*, pages 1151–1156. IEEE.
- Young, S. J. and Scheinerman, E. R. (2007). Random dot product graph models for social networks. In *International Workshop on Algorithms and Models for the Web-Graph*, pages 138–149. Springer.

- Yuan, M. and Wen, Q. (2021). A practical two-sample test for weighted random graphs. *Journal of Applied Statistics*, pages 1–17.
- Zhang, Y., Levina, E., and Zhu, J. (2017). Estimating network edge probabilities by neighbourhood smoothing. *Biometrika*, 104(4):771–783.
- Zhang, Y. and Xia, D. (2022). Edgeworth expansions for network moments. *The Annals of Statistics*, 50(2):726–753.

Supplementary Material to “Higher-order accurate two-sample network inference and network hashing”

S.1 Definitions and estimations of α 's and β 's in Section 3.2 of Main Paper

The Edgeworth expansion terms \mathcal{I}_0 , $Q_{m,n,\rho_A,\rho_B;1}$ and $Q_{m,n,\rho_A,\rho_B;2}$ depend on the expectation of quantities involving $\alpha_0, \dots, \alpha_4$ and β_0, \dots, β_4 , whose definitions are enumerated as follows. For completeness, we still write down the formulation of α_1 , which has been defined in Main Paper.

$$\alpha_0 := 2s(s+1)\rho_A^{-(s+2)}\mu_m\xi_{\rho_A;1}^2 - 2rs\rho_A^{-(s+1)}\xi_{A,\rho_A;1} \quad (\text{S1})$$

$$\alpha_1(X_i) := \rho_A^{-s} \cdot \{rg_{A;1}(X_i) - 2s\mu_m \cdot \rho_A^{-1} \cdot g_{\rho_A;1}(X_i)\} \quad (\text{S2})$$

$$\begin{aligned} \alpha_2(X_{i_1}, X_{i_2}) &:= \frac{r(r-1)}{2}\rho_A^{-s}g_{A;2}(X_{i_1}, X_{i_2}) - s\rho_A^{-(s+1)}\mu_m g_{\rho_A;2}(X_{i_1}, X_{i_2}) \\ &\quad + 2\rho_A^{-s}\mu_m s(s+1)\rho_A^{-2}g_{\rho_A;1}(X_{i_1})g_{\rho_A;1}(X_{i_2}) - 2rs\rho_A^{-(s+1)}g_{\rho_A;1}(X_{i_1})g_{A;1}(X_{i_2}) \end{aligned} \quad (\text{S3})$$

$$\begin{aligned} \alpha_3(X_i) &:= -4r^2s\rho_A^{-(2s+1)}\xi_{A;1}^2g_{\rho_A;1}(X_i) + r^2\rho_A^{-2s}(g_{A;1}^2(X_i) - \xi_{A;1}^2) \\ &\quad - 16s^2(s+1)\rho_A^{-(2s+3)}\mu_m^2\xi_{\rho_A;1}^2g_{\rho_A;1}(X_i) + 8rs^2\rho_A^{-(2s+2)}\mu_m g_{A;1}(X_i)\xi_{\rho_A;1}^2 \\ &\quad + 4s^2\rho_A^{-(2s+2)}\mu_m^2(g_{\rho_A;1}^2(X_i) - \xi_{\rho_A;1}^2) \\ &\quad - 4rs\left\{ - (4s+2)\rho_A^{-(2s+2)}g_{\rho_A;1}(X_i)\mu_m\xi_{A,\rho_A;1} + r\rho_A^{-(2s+1)}g_{A;1}(X_i)\xi_{A,\rho_A;1} \right. \\ &\quad \left. + \rho_A^{-(2s+1)}\mu_m(g_{A;1}(X_i)g_{\rho_A;1}(X_i) - \xi_{A,\rho_A;1}) \right\} \end{aligned} \quad (\text{S4})$$

$$\begin{aligned} \alpha_4(X_{i_1}, X_{i_2}) &:= 2r^2(r-1)\rho_A^{-2s}g_{A;1}(X_{i_1})g_{A;2}(X_{i_1}, X_{i_2}) + 8s^2\rho_A^{-(2s+2)}\mu_m^2 \\ &\quad g_{\rho_A;1}(X_{i_1})g_{\rho_A;2}(X_{i_1}, X_{i_2}) - 4r(r-1)s\rho_A^{-(2s+1)}\mu_m g_{\rho_A;1}(X_{i_1})g_{A;2}(X_{i_1}, X_{i_2}) \\ &\quad - 4rs\rho_A^{-(2s+1)}\mu_m g_{A;1}(X_{i_1})g_{\rho_A;2}(X_{i_1}, X_{i_2}). \end{aligned} \quad (\text{S5})$$

Similarly, define

$$\beta_0 := 2s(s+1)\rho_B^{-(s+2)}\nu_n\xi_{\rho_B;1}^2 - 2rs\rho_B^{-(s+1)}\xi_{B,\rho_B;1} \quad (\text{S6})$$

$$\beta_1(Y_i) := \rho_B^{-s} \cdot \{rg_{B;1}(Y_i) - 2s\nu_n \cdot \rho_B^{-1} \cdot g_{\rho_B;1}(Y_i)\} \quad (\text{S7})$$

$$\begin{aligned} \beta_2(Y_{i_1}, Y_{i_2}) &:= \frac{r(r-1)}{2}\rho_B^{-s}g_{B;2}(Y_{i_1}, Y_{i_2}) - s\rho_B^{-(s+1)}\nu_n g_{\rho_B;2}(Y_{i_1}, Y_{i_2}) \\ &\quad + 2\rho_B^{-s}\nu_n s(s+1)\rho_B^{-2}g_{\rho_B;1}(Y_{i_1})g_{\rho_B;1}(Y_{i_2}) - 2rs\rho_B^{-(s+1)}g_{\rho_B;1}(Y_{i_1})g_{B;1}(Y_{i_2}) \end{aligned} \quad (\text{S8})$$

$$\begin{aligned} \beta_3(Y_i) &:= -4r^2s\rho_B^{-(2s+1)}\xi_{B;1}^2g_{\rho_B;1}(Y_i) + r^2\rho_B^{-2s}(g_{B;1}^2(Y_i) - \xi_{B;1}^2) \\ &\quad - 16s^2(s+1)\rho_B^{-(2s+3)}\nu_n^2\xi_{\rho_B;1}^2g_{\rho_B;1}(Y_i) + 8rs^2\rho_B^{-(2s+2)}\nu_n g_{B;1}(Y_i)\xi_{\rho_B;1}^2 \\ &\quad + 4s^2\rho_B^{-(2s+2)}\nu_n^2(g_{\rho_B;1}^2(Y_i) - \xi_{\rho_B;1}^2) \\ &\quad - 4rs\left\{ - (4s+2)\rho_B^{-(2s+2)}g_{\rho_B;1}(Y_i)\nu_n\xi_{B,\rho_B;1} + r\rho_B^{-(2s+1)}g_{B;1}(Y_i)\xi_{B,\rho_B;1} \right. \end{aligned}$$

$$+ \rho_B^{-(2s+1)} \nu_n (g_{B;1}(Y_i) g_{\rho_B;1}(Y_i) - \xi_{B,\rho_B;1}) \} \quad (\text{S9})$$

$$\begin{aligned} \beta_4(Y_{i_1}, Y_{i_2}) := & 2r^2(r-1)\rho_B^{-2s} g_{B;1}(Y_{i_1}) g_{B;2}(Y_{i_1}, Y_{i_2}) + 8s^2 \rho_B^{-(2s+2)} \nu_n^2 \\ & g_{\rho_B;1}(Y_{i_1}) g_{\rho_B;2}(Y_{i_1}, Y_{i_2}) - 4r(r-1) s \rho_B^{-(2s+1)} \nu_n g_{\rho_B;1}(Y_{i_1}) g_{B;2}(Y_{i_1}, Y_{i_2}) \\ & - 4rs \rho_B^{-(2s+1)} \nu_n g_{B;1}(Y_{i_1}) g_{\rho_B;2}(Y_{i_1}, Y_{i_2}). \end{aligned} \quad (\text{S10})$$

All the above terms involve $g_{A;1}(\cdot)$, $g_{A;2}(\cdot, \cdot)$, $g_{\rho_A;1}(\cdot)$, $g_{\rho_A;2}(\cdot, \cdot)$ and $g_{B;1}(\cdot)$, $g_{B;2}(\cdot, \cdot)$, $g_{\rho_B;1}(\cdot)$, $g_{\rho_B;2}(\cdot, \cdot)$, which need to be estimated in practice. Without loss of generality, we only elaborate the estimators for all A -indexed quantities.

$$\widehat{g}_{A;1}(X_i) := \binom{m-1}{r-1}^{-1} \sum_{\{i_1 < \dots < i_{r-1}\} \subseteq [1:m] \setminus \{i\}} h(A_{i, i_1, \dots, i_{r-1}}) - \widehat{U}_m \quad (\text{S11})$$

$$\widehat{g}_{\rho_A;1}(X_i) := (m-1)^{-1} \sum_{1 \leq i' \leq m, i' \neq i} A_{ii'} - \widehat{\rho}_A \quad (\text{S12})$$

$$\widehat{g}_{A;2}(X_{i_1}, X_{i_2}) := \binom{m-2}{r-2}^{-1} \sum_{\substack{1 \leq i'_1 < \dots < i'_r \leq m \\ \{i_1, i_2\} \subseteq \{i'_1, \dots, i'_r\}}} h(A_{i, i'_1, \dots, i'_r}) - \widehat{g}_{A;1}(X_{i_1}) - \widehat{g}_{A;1}(X_{i_2}) - \widehat{U}_m \quad (\text{S13})$$

$$\widehat{g}_{\rho_A;2}(X_{i_1}, X_{i_2}) := A_{i_1 i_2} - \widehat{g}_{\rho_A;1}(X_{i_1}) - \widehat{g}_{\rho_A;1}(X_{i_2}) - \widehat{\rho}_A \quad (\text{S14})$$

Then, $\xi_{A;1}^2$ and $\xi_{A,\rho_A;1}$ can be estimated, respectively, by

$$\widehat{\xi}_{A;1}^2 := \frac{1}{m} \sum_{i=1}^m \{\widehat{g}_{A;1}(X_i)\}^2 \quad \text{and} \quad \widehat{\xi}_{A,\rho_A;1} := \frac{1}{m} \sum_{i=1}^m \widehat{g}_{A;1}(X_i) \widehat{g}_{\rho_A;1}(X_i) \quad (\text{S15})$$

Similarly, define $\widehat{\xi}_{\rho_A;1}^2 := m^{-1} \sum_{i=1}^m \widehat{g}_{\rho_A;1}^2(X_i)$. Plug the estimates \widehat{U}_m , $\widehat{\rho}_A$, $\widehat{\xi}_{A;1}^2$, $\widehat{\xi}_{\rho_A;1}^2$, $\widehat{\xi}_{A,\rho_A;1}$, $\widehat{g}_{A;1}(\cdot)$, $\widehat{g}_{A;2}(\cdot, \cdot)$, $\widehat{g}_{\rho_A;1}(\cdot)$, $\widehat{g}_{\rho_A;2}(\cdot, \cdot)$ into eq. (S1) through (S5). We can now define the empirical estimates $\widehat{\alpha}_0$, $\widehat{\alpha}_1(X_i)$, $\widehat{\alpha}_2(X_{i_1}, X_{i_2})$, $\widehat{\alpha}_3(X_i)$ and $\widehat{\alpha}_4(X_{i_1}, X_{i_2})$, e.g., $\widehat{\alpha}_1(X_i) := r \widehat{\rho}_A^{-s} \widehat{g}_{A;1}(X_i) - 2s \widehat{\rho}_A^{-(s+1)} \widehat{U}_m \widehat{g}_{\rho_A;1}(X_i)$. Moreover, we estimate $\sigma_{m,n}^2$ by

$$\widehat{S}_{m,n}^2 := \frac{1}{m^2} \sum_{i=1}^m \widehat{\alpha}_1^2(X_i) + \frac{1}{n^2} \sum_{j=1}^n \widehat{\beta}_1^2(Y_j).$$

Equipped with above estimates $\widehat{S}_{m,n}^2$, $\widehat{\alpha}_0$, $\widehat{\alpha}_1(X_i)$, $\widehat{\alpha}_2(X_{i_1}, X_{i_2})$, $\widehat{\alpha}_3(X_i)$ and $\widehat{\alpha}_4(X_{i_1}, X_{i_2})$, the empirical version of the Edgeworth expansion terms $\widehat{\mathcal{I}}_0$, $\widehat{Q}_{m,n,\rho_A,\rho_B;1}$ and $\widehat{Q}_{m,n,\rho_A,\rho_B;2}$ can be calculated accordingly. For instance,

$$\widehat{\mathcal{I}}_0 := \widehat{S}_{m,n}^{-1} (m^{-1} \widehat{\alpha}_0 - n^{-1} \widehat{\beta}_0), \quad (\text{S16})$$

and we formulate $\widehat{Q}_{m,n,\rho_A,\rho_B;1}$ and $\widehat{Q}_{m,n,\rho_A,\rho_B;2}$ exactly similarly, but we omit the display of their lengthy expressions. Note that the expectations $\mathbb{E}[\alpha_1^3(X_1)]$, $\mathbb{E}[\alpha_1(X_1)\alpha_3(X_1)]$, $\mathbb{E}[\alpha_4(X_1, X_2)\alpha_1(X_2)]$ and $\mathbb{E}[\alpha_1(X_1)\alpha_1(X_2)\alpha_2(X_1, X_2)]$ are all calculated by the empirical version, e.g.,

$$\widehat{\mathbb{E}}[\alpha_1^3(X_1)] := \frac{1}{m} \sum_{i=1}^m \widehat{\alpha}_1^3(X_i) \quad (\text{S17})$$

$$\widehat{\mathbb{E}}[\alpha_1(X_1)\alpha_1(X_2)\alpha_2(X_1, X_2)] := \binom{m}{2}^{-1} \sum_{1 \leq i_1 < i_2 \leq m} \widehat{\alpha}_1(X_{i_1})\widehat{\alpha}_1(X_{i_2})\widehat{\alpha}_2(X_{i_1}, X_{i_2}). \quad (\text{S18})$$

Additionally, $\xi_{\alpha;1}^2$ and $\xi_{\beta;1}^2$ can be estimated via

$$\widehat{\xi}_{\alpha;1}^2 = \frac{1}{m} \sum_{i=1}^m \widehat{\alpha}_1(X_i)^2 \quad \text{and} \quad \widehat{\xi}_{\beta;1}^2 = \frac{1}{n} \sum_{j=1}^n \widehat{\beta}_1(Y_j)^2. \quad (\text{S19})$$

S.2 Additional simulation set-up information and results

S.2.1 Addition simulation results for Simulation 2 in Section 5.2 in Main Paper

Tables S1 – S8 show the numerical results of empirical 90% CI coverage probabilities of our method and $N(0, 1)$ approximation. The purpose of displaying these tables is to provide more details and confirm the marginal accuracy of our method, completing the message conveyed by Figure 2 in Main Paper.

Table S1: Empirical CI coverage probabilities, level = 90%, Triangle, our method, Mean(SD)

Network sizes	$n = 10$	$n = 20$	$n = 40$	$n = 80$	$n = 160$
$m = 10$	0.671(0.470)	0.672(0.470)	0.669(0.470)	0.668(0.471)	0.674(0.469)
$m = 20$	0.862(0.344)	0.860(0.347)	0.857(0.350)	0.859(0.348)	0.858(0.349)
$m = 40$	0.895(0.307)	0.895(0.306)	0.894(0.307)	0.894(0.308)	0.897(0.304)
$m = 80$	0.898(0.303)	0.903(0.295)	0.902(0.297)	0.899(0.301)	0.901(0.299)
$m = 160$	0.890(0.313)	0.907(0.290)	0.905(0.294)	0.903(0.296)	0.902(0.297)

Table S2: Empirical CI coverage probabilities, level = 90%, Vshape, our method, Mean(SD)

Network sizes	$n = 10$	$n = 20$	$n = 40$	$n = 80$	$n = 160$
$m = 10$	0.872(0.334)	0.876(0.329)	0.877(0.328)	0.877(0.328)	0.877(0.328)
$m = 20$	0.909(0.288)	0.914(0.281)	0.913(0.282)	0.912(0.283)	0.914(0.281)
$m = 40$	0.907(0.290)	0.920(0.272)	0.919(0.273)	0.918(0.274)	0.920(0.271)
$m = 80$	0.893(0.309)	0.917(0.276)	0.915(0.279)	0.912(0.283)	0.913(0.282)
$m = 160$	0.874(0.332)	0.916(0.278)	0.912(0.283)	0.909(0.287)	0.908(0.289)

S.2.2 Detailed simulation set-up information and full-X-range plots for Simulation 3 in Section 5.3 in Main Paper

In the simulation, we generated a large network database with 10 different graphon models, listed as follows. All these graphons' $f(\cdot, \cdot)$ functions have been rescaled such that $\int_{[0,1]^2} f(u, v) du dv = 1$. Set $\rho_A = \rho_{B_1} = \dots = \rho_{B_K} = 0.4$.

Table S3: Empirical CI coverage probabilities, level = 90%, Triangle, subsample, Mean(SD)

Network sizes	$n = 10$	$n = 20$	$n = 40$	$n = 80$	$n = 160$
$m = 10$	0.749(0.434)	0.693(0.461)	0.663(0.473)	0.643(0.479)	0.623(0.485)
$m = 20$	0.825(0.380)	0.803(0.398)	0.758(0.428)	0.745(0.436)	0.734(0.442)
$m = 40$	0.845(0.362)	0.836(0.370)	0.814(0.389)	0.807(0.394)	0.806(0.395)
$m = 80$	0.839(0.368)	0.826(0.379)	0.790(0.408)	0.790(0.407)	0.785(0.411)
$m = 160$	0.875(0.331)	0.825(0.380)	0.766(0.424)	0.769(0.422)	0.775(0.418)

Table S4: Empirical CI coverage probabilities, level = 90%, Vshape, subsample, Mean(SD)

Network sizes	$n = 10$	$n = 20$	$n = 40$	$n = 80$	$n = 160$
$m = 10$	0.784(0.411)	0.726(0.446)	0.689(0.463)	0.678(0.467)	0.670(0.470)
$m = 20$	0.751(0.432)	0.697(0.460)	0.672(0.469)	0.670(0.470)	0.672(0.470)
$m = 40$	0.762(0.426)	0.686(0.464)	0.692(0.462)	0.699(0.459)	0.707(0.455)
$m = 80$	0.792(0.406)	0.694(0.461)	0.694(0.461)	0.710(0.454)	0.719(0.450)
$m = 160$	0.850(0.357)	0.716(0.451)	0.707(0.455)	0.726(0.446)	0.739(0.439)

Table S5: Empirical CI coverage probabilities, level = 90%, Triangle, resample, Mean(SD)

Network sizes	$n = 10$	$n = 20$	$n = 40$	$n = 80$	$n = 160$
$m = 10$	0.835(0.371)	0.849(0.358)	0.855(0.352)	0.854(0.353)	0.856(0.351)
$m = 20$	0.847(0.360)	0.877(0.329)	0.889(0.314)	0.894(0.308)	0.894(0.308)
$m = 40$	0.841(0.366)	0.867(0.339)	0.888(0.315)	0.892(0.311)	0.895(0.306)
$m = 80$	0.846(0.361)	0.862(0.345)	0.887(0.317)	0.890(0.313)	0.893(0.309)
$m = 160$	0.857(0.350)	0.855(0.352)	0.887(0.316)	0.893(0.309)	0.895(0.307)

Table S6: Empirical CI coverage probabilities, level = 90%, Vshape, resample, Mean(SD)

Network sizes	$n = 10$	$n = 20$	$n = 40$	$n = 80$	$n = 160$
$m = 10$	0.636(0.481)	0.685(0.465)	0.688(0.463)	0.682(0.466)	0.679(0.467)
$m = 20$	0.728(0.445)	0.784(0.411)	0.780(0.414)	0.771(0.420)	0.762(0.426)
$m = 40$	0.780(0.414)	0.834(0.372)	0.847(0.360)	0.831(0.375)	0.824(0.381)
$m = 80$	0.798(0.401)	0.850(0.357)	0.879(0.326)	0.867(0.339)	0.858(0.349)
$m = 160$	0.797(0.402)	0.842(0.364)	0.890(0.312)	0.890(0.313)	0.880(0.325)

Table S7: Empirical CI coverage probabilities, level = 90%, Triangle, $N(0, 1)$, Mean(SD)

Network sizes	$n = 10$	$n = 20$	$n = 40$	$n = 80$	$n = 160$
$m = 10$	0.694(0.461)	0.676(0.468)	0.672(0.469)	0.672(0.469)	0.673(0.469)
$m = 20$	0.866(0.340)	0.831(0.375)	0.819(0.385)	0.820(0.384)	0.819(0.385)
$m = 40$	0.925(0.264)	0.879(0.326)	0.868(0.339)	0.862(0.345)	0.865(0.342)
$m = 80$	0.948(0.221)	0.904(0.294)	0.889(0.314)	0.883(0.322)	0.884(0.320)
$m = 160$	0.953(0.211)	0.918(0.274)	0.900(0.300)	0.893(0.309)	0.891(0.312)

Table S8: Empirical CI coverage probabilities, level = 90%, Vshape, $N(0, 1)$, Mean(SD)

Network sizes	$n = 10$	$n = 20$	$n = 40$	$n = 80$	$n = 160$
$m = 10$	0.828(0.377)	0.801(0.399)	0.795(0.403)	0.795(0.404)	0.796(0.403)
$m = 20$	0.914(0.280)	0.865(0.341)	0.853(0.354)	0.853(0.354)	0.851(0.356)
$m = 40$	0.960(0.195)	0.902(0.297)	0.887(0.316)	0.882(0.323)	0.883(0.321)
$m = 80$	0.971(0.168)	0.922(0.268)	0.901(0.299)	0.893(0.309)	0.894(0.308)
$m = 160$	0.960(0.196)	0.936(0.244)	0.909(0.288)	0.901(0.299)	0.898(0.302)

1. SmoothGraphon-1: $f(u, v) = u + v$;
2. SmoothGraphon-2: $f(u, v) = (u + v)^2/2 \cdot \tau$, where $\tau = 1.71$;
3. SmoothGraphon-3: $f(u, v) = e^{-(u+v)/2} \cdot \tau$, where $\tau = 1.61$;
4. SmoothGraphon-4: $f(u, v) = e^{-(u+v)/3} \cdot \tau$, where $\tau = 1.38$;
5. SmoothGraphon-5: $f(u, v) = \cos((u + v)/2) \cdot \tau$, where $\tau = 1.16$; $\cos(1/(u^2 + v^2)) + 0.15 \cdot \tau$, where $\tau = 4.57$;
6. BlockModel-1: Stochastic block model with $K = 2$ equal-sized communities and edge probabilities $B = (0.6, 0.2; 0.2, 0.2) \cdot \tau$, where $\tau = 3.33$;
7. BlockModel-2: Stochastic block model with $K = 2$ equal-sized communities and edge probabilities $B = (0.4, 0.1; 0.1, 0.1) \cdot \tau$, where $\tau = 5.71$;
8. BlockModel-3: Stochastic block model with $K = 2$ with $(3/4, 1/4)$ sized communities and edge probabilities $B = (0.6, 0.2; 0.2, 0.2) \cdot \tau$, where $\tau = 2.35$;
9. BlockModel-4: Stochastic block model with $K = 2$ with $(1/3, 2/3)$ sized communities and edge probabilities $B = (0.8, 0.4; 0.4, 0.2) \cdot \tau$, where $\tau = 2.81$;
10. BlockModel-5: Stochastic block model with $(2/3, 1/3)$ sized communities and edge probabilities $B = (0.8, 0.2; 0.2, 0.2) \cdot \tau$, where $\tau = 2.14$.

The two keyword networks are generated from the following graphon models:

- Keyword 1: Same as BlockModel-1.
- Keyword 2: SmoothGraphon-6: $f(u, v) := \{(u^2 + v^2)/3 \cdot \cos(1/(u^2 + v^2)) + 0.15\} \cdot \tau$, where $\tau = 4.57$.

Figure S1 shows full- X -range plots of Row 2 in Figure 3 in Main Paper, with two more cases $n = 200$, $n = 800$, both omitted in Main Paper to meet page limit. Particularly, the $n = 1600$ plot in Figure S1 better matches the interpretation at the end of the second paragraph in Section ?? in Main Paper, that there should be some cyan bars to the left of $\log(5\%)$ reference line, showing not-match.

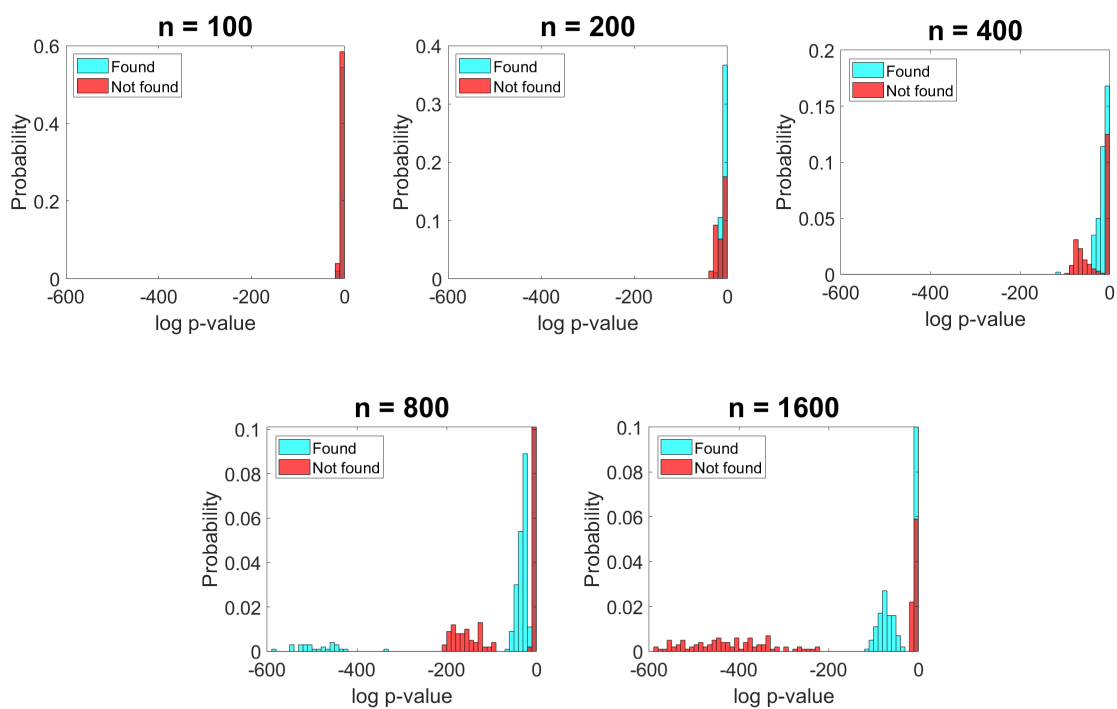


Figure S1: Histograms of p-values from queries keyword 1 vs database (“found”, cyan) and keyword 2 vs database (“not found”, red), full-X-range plots for Row 2 of Figure 3 in Main Paper.